Development of timber buckling-restrained braces for mass timber braced frames

Colton Murphy, University of Utah
Chris Pantelides. University of Utah
Hans-Erik Blomgren, Katerra
Douglas Rammer, Forest Products Laboratory

Keywords: brace, buckling, building, damping, frame, fuse, seismic, structure, timber.

1 Abstract

Buckling Restrained Brace Frames (BRBF) are a proven and reliable method to provide an efficient lateral force resisting system for new and existing structures in earthquake prone regions. The fuse-type elements in this system facilitate stable energy dissipation at large load deformation levels. Currently, the new trend towards mass timber vertical structures creates a need for a lightweight compatible lateral force resisting system. A Buckling Restrained Brace (BRB) component is possible to construct and feasible to implement when combining a steel core with a mass timber casing herein named the Timber-Buckling Restrained Brace (T-BRB). T-BRBs when combined with mass timber beam and column elements can create a system that will have advantages over the current steel framed BRBF system when considering recyclability, sustainability, framing compatibility, and performance. This paper presents findings on small scale testing of candidate engineered wood products for the T-BRB casing and testing of six full scale 12 ft long 60 kip braces according to code prescribed loading protocols and acceptance criteria.

2 Introduction & Motivation

Research has proven that Buckling Restrained Braces provide satisfactory stiffness, strength and stable energy dissipation (Black et al. 2004). These braces also provide adequate rigidity necessary to satisfy building interstory drift limits. The manufacturing of lightweight and economical fuse-type BRBs are important for ease of handling during construction. Recent advancements in timber technology is making multi-story mass

timber buildings an attractive option to replace traditional steel and concrete systems. Mass timber buildings attract less seismic inertial forces, however, they lack code defined lateral force resisting systems (Blomgren et al. 2016); the authors proved that a buckling restrained brace with a Glulam casing can be built which exhibits superior qualities when compared to conventional dowel end timber braces. The T-BRB exhibited higher axial load, higher stiffness, more stable axial deformation capacity, and significantly greater energy dissipation characteristics when compared to conventional timber braces. Ductility and seismic damping of conventional timber braces is a concern in high seismic regions and extra care should be taken in the design of the connections to reach high ductility demands during an earthquake (Popovski 2000). Issues with conventional timber brace connections include ductility and consistency of performance regarding strength and stiffness.

3 T-BRB Design Methodology

Design of the casing dimensions used Euler buckling principles to avoid global brace buckling (Watanabe et al. 1988). Research aimed at exploring the high-mode buckling responses of the BRB core plates by Wu et al. (2013) was used for the design of the core and understanding of the internal modal responses of the T-BRB. Methods to design the casing bolts were developed which resist both the weak and strong axis core buckling forces. The bulging force from the weak axis core buckling can be predicted and prevented using adequate casing design (Lin et al. 2011). Gaps present between the core and casing can diminish the ability of the BRB to dissipate energy in compression (Genna and Gelfi 2012) by exacerbating lateral casing thrusts and making internal forces difficult to predict.

To inform the design, various types of small-scale timber block specimens were tested to determine mechanical properties that would be beneficial for a T-BRB casing. Wood type, screw reinforcement and direction of load, parallel or perpendicular to lamination, were considered as variables. Screw reinforcement in timber can promote load transfer and can compensate for wood with low compressive strength when loaded perpendicular to grain (Blass and Bejtka 2003). The anisotropic nature of engineered timber and wood in general leads to non-uniform load distribution. Experimentation into dowel connections showed both underestimation and overestimation in strength and stiffness when using a simplified calculation approach (Bader et al. 2016).

4 Small Scale Block Tests

The strength and stiffness of various mass timber engineered wood products under certain loading conditions is not well known. In addition, the influence of compression screw perpendicular to grain reinforcement on the mechanical behavior is also not well known. The localized compressive strength and stiffness under concentrated loads of Laminated Veneer Lumber (LVL), Parallel Strand Lumber (PSL), Glued laminated timber (Glulam), and Mass Plywood Panel (MPP) are investigated.

4.1 Block Test Program

The compressive tests conducted included both monotonic and cyclic tests. All mass timber specimens were 6in.x6in.x12in. Select specimens were loaded both perpendicular and parallel to the wood grain of their laminations. Additional specimens were tested with perpendicular to grain compression screws used for reinforcement. The reinforced specimens included four 3/8in. diameter x 4 in. screws spaced in a 2in.x2in. square pattern. A 3in.x3in. steel fixed head platen was used to apply the vertical compressive load to the face of the specimen. Two replicates of each type of test were carried out. Alternative tests focusing on glulam were carried out; this included adjusting the screw pattern to 2in.x3in., and 2in.x4in. along with adjusting the platen dimensions to 3in.x4in., and 3in.x5in., respectively. These four additional trials used the quasi-static cyclic load protocol shown in Fig. 1, which was continued until critical failure. The cyclic load protocol used a loading rate of 1 cycle per second. The monotonic loading protocol, also shown in Fig. 1, is a quasi-static, linear compressive load; this load was also continued until failure. Fig. 2 shows the typical 2in.x2in. screw reinforcement after being loaded to failure from the 3in.x3in. platen. Figure 2 also shows an unreinforced glulam specimen loaded to failure in the parallel to lamination direction.

4.2 Block Test Results

Figures 3 and 4 represent a sample of the load versus displacement plots from the monotonic tests conducted. These figures display data from the monotonic tests perpendicular to the laminations and parallel to the laminations both with and without reinforcement. The nomenclature is as follows: M=MPP, G=Glulam, P=PSL, L=LVL, A=parallel to lamination, B=perpendicular to lamination, U= unreinforced. These figures clearly show the improved stiffness and maximum load when compressing MPP parallel to the laminations. These figures also show an increased stiffness when applying load parallel to the laminations. Figure 5 provides cyclic test samples for each wood type and

configuration. These cyclic tests show MPP loaded perpendicular to lamination has a lower yield force when compared to parallel to lamination, however it has a hardening characteristic and exhibits more ductility. Unreinforced Glulam underperforms when compared to other engineered wood products tested; this wood type consistently fails before reaching 0.1in. MPP loaded perpendicular to laminations and without screw reinforcement also underperforms compared to MPP loaded parallel to laminations.

Research in T-BRBs identified that a high elastic stiffness with a high maximum compressive load capacity is desirable for a T-BRB casing (Blomgren et al 2016). If the modulus of elasticity of the casing is too low, localized weak axis buckling occurs which leads to premature failure. Higher elastic stiffness of the casing suppresses high mode weak axis buckling throughout the length of the core, which is desirable. Unreinforced MPP loaded parallel to the laminations outperformed LVL, PSL, and Glulam. The fact that screw reinforcement is not necessary to maintain good results, brings economy in materials and labor to the manufacturing process of the braces.

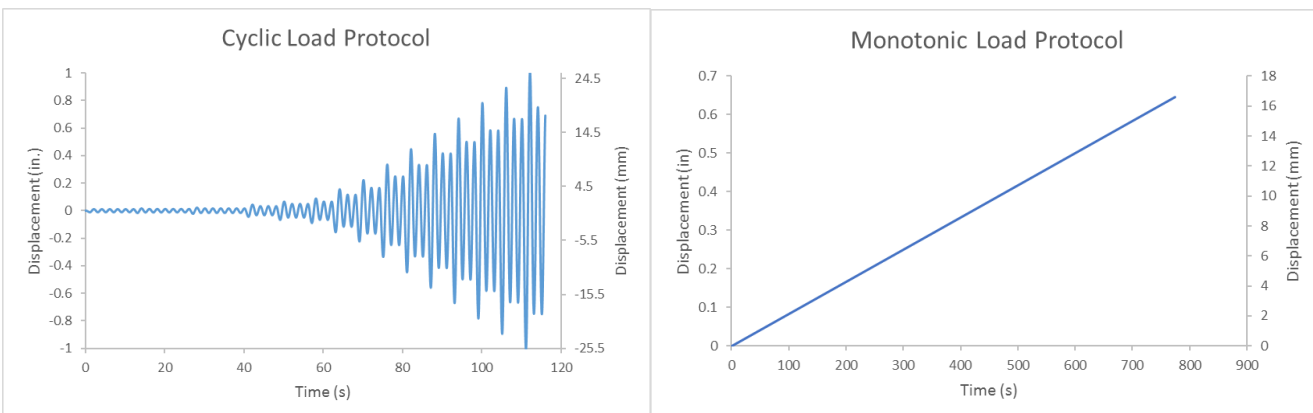

Figure 1. Block Specimen Load protocols.

(a) (b)

Figure 2. Glulam specimens post-test: (a) no screw reinforcement; (b) 2 in. x 2 in. reinforcement.

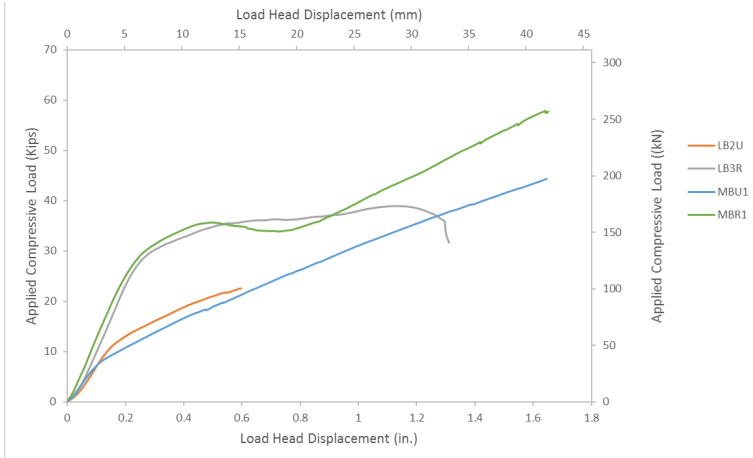

Figure 3. Sample of specimens loaded monotonically and perpendicular to lamination.

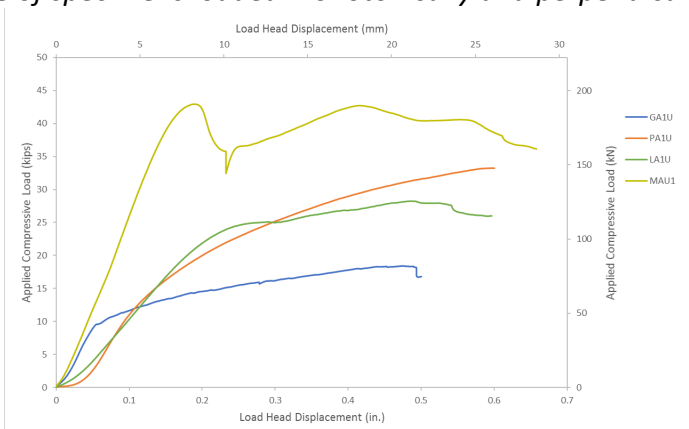

Figure 4. Sample of specimens loaded monotonically and parallel to lamination without reinforcement.

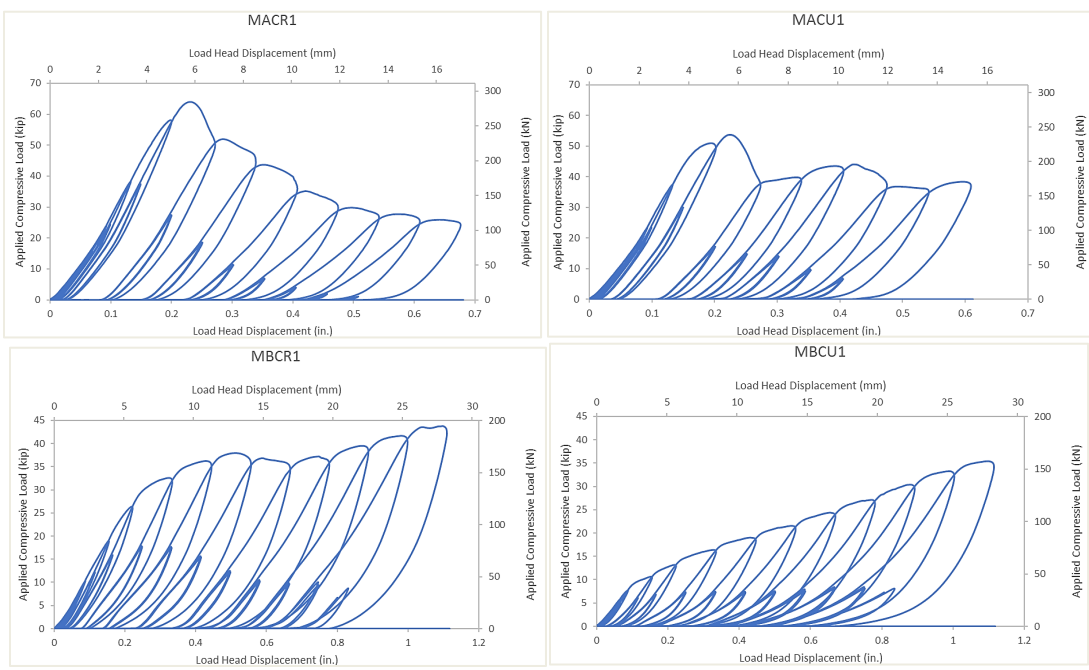

Figure 5. Individual cyclic test sample hysteresis curves.

5 T-BRB Full Scale Element Tests

T-BRBs act as a structural fuse dissipating energy by yielding the steel core and thus protecting the beam and column elements of the braced frame system during a seismic event. Six full scale, 12-ft long, T-BRBs were constructed and tested under cyclic axial load in this research. The first three T-BRBs were loaded using a fatigue-based load protocol in which a high number of cycles was applied at significant steel core strain. The final three T-BRBs were loaded using a drift-based load protocol in which higher steel core strain cycles were applied until failure.

5.1 T-BRB Specimens

The six T-BRBs were constructed using 41ksi yield strength steel cores and mechanically fastened Mass Plywood Panel (MPP) casings as shown in Fig. 6. Figure 7 (left) shows an exploded view of the T-BRB components. In order to increase ductility and improve overall performance a low yielding steel core was chosen. The stiffener plates at each end of the core plate are fabricated with the same steel. The design value for yield strength was taken as 41ksi and tensile ultimate strength was taken as 62.5ksi. The core cross-sectional dimensions along the yield zone are 3in.x0.5in. to form a 1.5in.^{2} yield area. The stiffener plates were welded to the core to prevent localized buckling outside of the timber casing. Two cheek plates were also welded to the ends of the T-BRBs around the pin connection to prevent a tear out failure. A steel dowel was welded to the core at mid-length to encourage an even distribution of core buckling forces.

Hardwood spacers were used to restrain strong axis buckling of the core plate. A laminated German beech wood material was used for the spacer. The material was cut to the exact dimensions necessary to fill the void made by the steel core between the timber casing material. Several ½in. diameter, A449 thru bolts were used to connect the two MPP casing elements; these bolts are also used to secure the hardwood spacers. A 7in. spacing of the bolts was used throughout the yielding length of the T-BRB; however, this spacing was reduced near the ends of the T-BRB to account for an increase in bending forces that were predicted. The 7in. bolt spacing throughout the yielding zone is a conservative estimate based on the calculations in Eqs. (1) and (2) and using the Fig. 7 (right) free body diagram of the buckled core inside of the casing.

$$\Delta_{gap} = v\varepsilon_{max}t_f \quad (1)$$

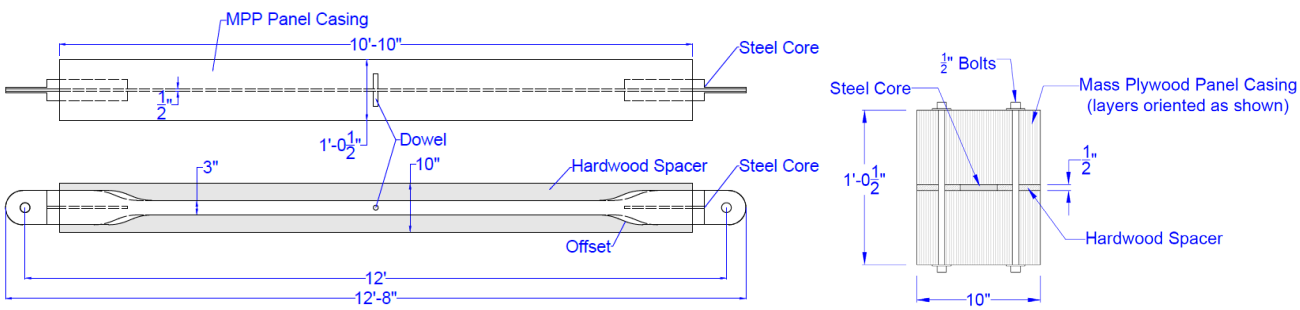

Figure 6. T-BRB Layout (bolts not shown).

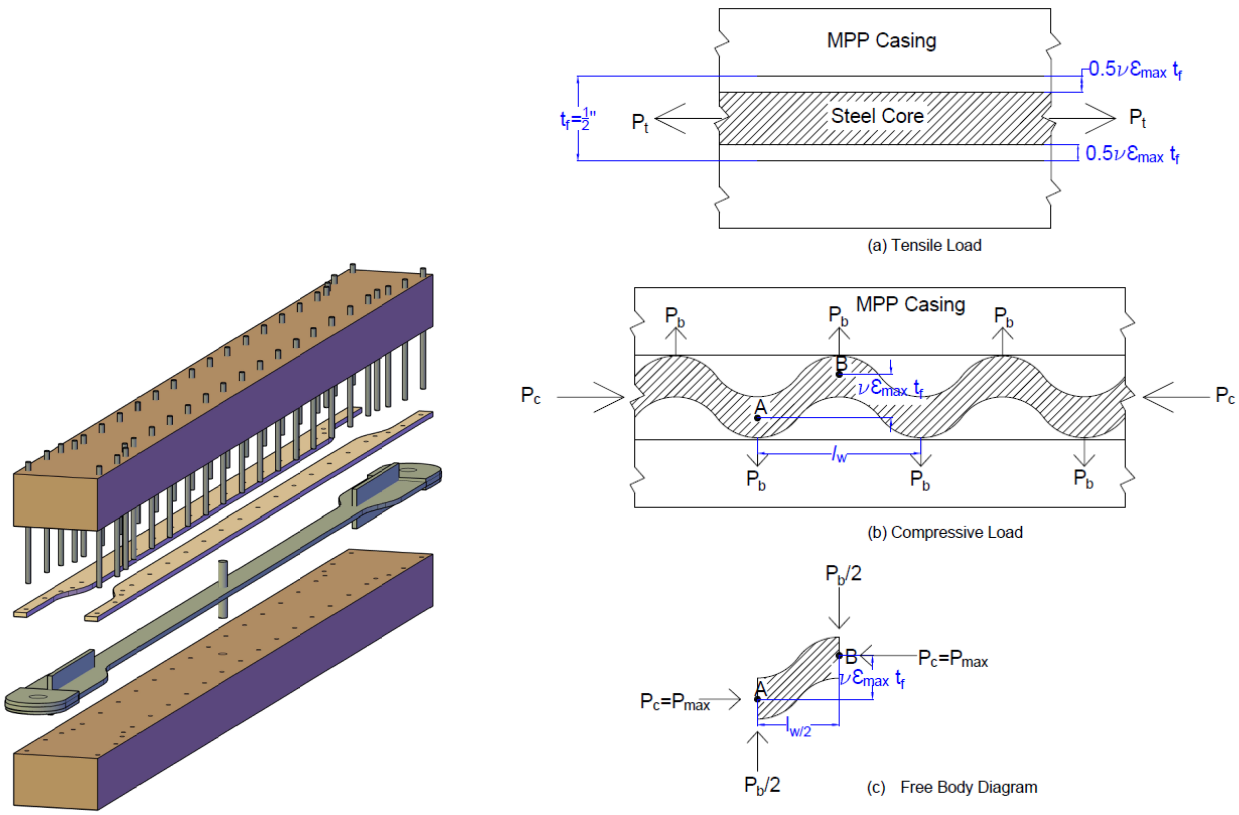

Figure 7. Exploded view visualization of the T-BRB design (left) and internal mechanics of buckling T-BRB (right).

The original steel core thickness, t_f, is ½in. Once the steel core goes into tension, a gap forms between the steel and the timber casing of increasing magnitude throughout the cyclic test due to Poisson effect. A Poisson's ratio, ν, of 0.5 was used for the steel core, which would be subject to high strains and would be in the plastic region. This gap is equal to Δ_{gap} in Eq. (1); ε_{max} is the maximum tensile strain in the steel during the test and is assumed to be 0.04. The wavelength of the buckled steel core, l_w, is assumed to be 11 times the thickness of the steel core (Wu et al. 2013) or 5.5in. P_{max} is the estimated maximum compressive force developed by the T-BRB; this value was estimated as 1.6 times the yield strength of the steel core to account for hardening and friction. A value

of 100kips was used for P_{max}. By summing the moments in the free body diagram of Fig. 7 (right) and solving for P_b, the buckling force of the steel core, Eq. (2) is formed:

$$P_b = \frac{4P_{max}\nu\varepsilon_{max}t_f}{l_w} \quad (2)$$

By solving Eq. (2), P_b is 727lbs. This value was rounded up to 1000lbs to apply a safety factor of 1.4. This force is exerted onto the core throughout the yield length a total of 36 times due to the 5.5 in. wavelength spacing. This results in a total casing outward force of 36 kips. By allocating 1.5 kips of allowable force per bolt, which factors in bolt prestressing strength loss during the pneumatic torque tightening process, 24 A449 bolts with ½in. diameter are needed throughout the yield length of the core. The 7in. bolt spacing provides 28 bolts throughout the 98in. yield zone. The design also satisfies the T-BRB global buckling capacity based on the National Design Specification for wood construction section for built up mechanically laminated timber columns (ANSI/AWC 2018). This spacing is conservative; failure involving bolt fracture was avoided during design so the failure modes of interest could be observed during testing.

Three layup grades of MPP panels were used in the six T-BRB tests. Each 10in. thick MPP plywood layup utilized a varying elastic modulus of $1.0\text{x}10^6$psi or $2.2\text{x}10^6$psi layers. The three MPP casing types are denoted as soft (s), medium (m), and hard (h). Figure 8 represents the lamination layup for the three MPP specimen types. The soft specimens consisted of four center 1in. thick laminations of $1.0\text{x}10^6$psi plywood with three outer laminations on each side of $2.2\text{x}10^6$psi plywood as shown in Fig. 8(a). The medium specimens contained only two 1in. laminations of $1.0\text{x}10^6$psi with the remaining laminations made of $2.2\text{x}10^6$psi plywood as shown in Fig. 8(b). The hard specimens were made entirely of $2.2\text{x}10^6$psi laminations as shown in Fig. 8(c). Specimens 1-3 were soft, medium, and hard, respectively; specimens 4-6 were hard, medium, and soft respectively.

5.2 T-BRB Loading Program

Two loading protocols were used for the six T-BRB experiments: fatigue-based and drift-based. The fatigue-based cyclic loading protocol was developed using AISC 341 (AISC 2016) Chapter F4 and Appendix K3. Since the experiment is uniaxial with pin end connections, a subassemblage test was not performed. Cyclic drift was increased by 0.5% until a 2% drift ratio was reached; subsequently the drift ratio was reduced to 1.5%. Finally, the 1.5% drift ratio was cycled until failure. In the drift-based loading protocol, the T-BRB drift was increased by 0.5% until failure with these steps: 0.5%, 1.0%, 1.5%, 2.0%, 2.5%, and 3.0%. A 98in. yield zone was used to calculate strain and axial displacement.

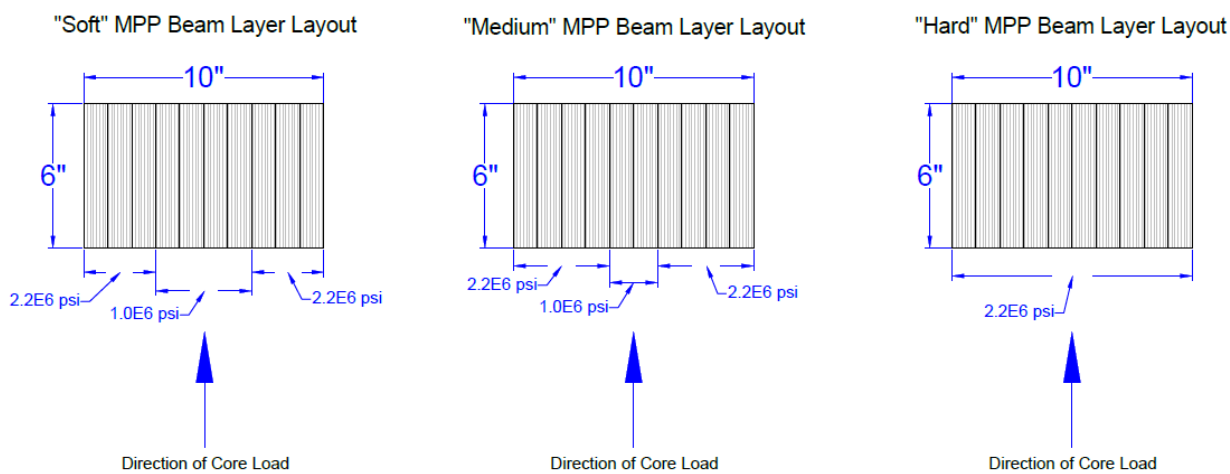

(a) (b) (c)

Figure 8. MPP layup detail for the three specimen casing types.

AISC 341-16 requires the brace to be tested to the design story drift and to achieve a Cumulative Inelastic Deformation (CID) of 200 times the yield deformation. The design story drift, Δ_{bm}, and the brace yield deformation, Δ_{by}, were determined as follows. The value of Δ_{bm} was calculated as 1.00% which is 1.28 in. The value of Δ_{by} was calculated using the following equations:

$$\Delta_{b-ysc} = \frac{F_{ysc}L_{ysc}}{E} \tag{3}$$

$$\Delta_{b-ends} = 2\frac{A_{sc}}{A_{end}}\left(\frac{F_{ysc}L_{end}}{E}\right) \tag{4}$$

$$\Delta_{by} = \Delta_{b-ysc} + \Delta_{b-end} + \Delta_{apparatus} \tag{5}$$

The value of $\Delta_{apparatus}$ was taken as zero due to the details of the instrumentation; F_{ysc} is the yield strength of the steel; L_{ysc} is the length of the yield zone; A_{sc} is the area of the yield zone; A_{end} is the area of the end of the T-BRB core which includes the stiffeners and cheek plates; L_{end} is the length of the ends of the core excluded by the yield zone. The brace yield deformation Δ_{by} was determined to be equal to 0.16 in. CID was calculated per AISC 341-16 table C-K3.1. CID is the accumulation of deformation, both positive and negative, beyond yield which is then converted multiples of brace yield deformation, Δ_{by}. The adjustment factors were determined using the hysteresis curves shown in Figs. 12-17. The compressive adjustment factor β was calculated using:

$$1.00 < \beta = \frac{P_{max}}{T_{max}} < 1.50 \tag{6}$$

β is the ratio between the maximum measured compressive load and the maximum measured tensile load per loading cycle, which should remain below 1.5 per AISC 341-16. The strain hardening adjustment factor was calculated using the following equation:

$$\omega = \frac{T_{max}}{R_y P_{ysc}} \geq 1.00 \quad (7)$$

ω is the ratio between the maximum measured tensile load and the yield force per cycle. Because coupon tests were conducted to determine yield stress, R_y is equal to 1.0.

5.3 T-BRB Test Results

Table 1 represents a summary of results from the six T-BRB tests. Hysteresis curves along with time-displacement figures for the six specimens are provided in Figs. 9-12. All hysteresis curves remained stable throughout each test. Figures 13-15 show images of the failure in each test.

Specimen 1 failed in tension at 39 cycles; the steel core fractured due to low cycle fatigue and the compressive adjustment factor, β, ranged from 1.05 to 1.20; the strain hardening adjustment factor ω ranged from 1.00 to 1.40. Specimen 2 failed in compression at 35 cycles; the MPP layers ruptured due to high compression transferred from the steel core, which buckled about the weak axis; β, ranged from 1.05 to 1.15; ω ranged from 1.00 to 1.32. Specimen 3 failed in compression at 28 cycles; failure was similar to specimen 2 because the MPP layers ruptured due to the load demand from the weak axis buckling of the steel core; β, ranged from 1.03 to 1.20; ω ranged from 1.00 to 1.35.

Specimen 4 failed in compression on the 13th cycle at 3.92% strain; slight strong axis buckling of the steel core was visible after inspection, but weak axis buckling was dominant and the ultimate failure mode was a ruptured casing; β, ranged from 1.04 to 1.23 and ω ranged from 1.00 to 1.43. Specimen 5 failed in compression on the 12th cycle at 3.92% strain; both weak- and strong-axis buckling of the steel core were present and the ultimate failure mode was a ruptured and split casing; β, ranged from 1.10 to 1.20 and ω ranged from 1.00 to 1.38. Specimen 6 failed on the 13th cycle at 3.92% strain;

Table 1. Results summary for T-BRB tests cycled to failure.

Protocol Type	Specimen Order #	MPP Layout Stiffness	Max % Strain	Max % Drift	Cycles to Failure	CID	Total Hysteretic Energy Dissipation (kip*in.)
Fatigue	1	soft	2.61%	2.00%	39	1571	19422
	2	medium	2.61%	2.00%	35.5	1416	16840
	3	hard	2.61%	2.00%	28.5	1107	13161
Drift	4	hard	3.92%	3.00%	13.5	580	7140
	5	medium	3.92%	3.00%	12.5	488	6379
	6	soft	3.92%	3.00%	13.5	580	7188

weak- and strong-axis buckling of the steel core were present, however strong-axis buckling of the steel core was severe and dominant. The casing layers split and opened due to the strong axis buckling force; β, ranged from 1.11 to 1.25 and ω ranged from 1.00 to 1.41. The load transferred to the MPP from strong axis steel core buckling in specimens 4-6 worked to pull apart plywood laminations. This cross-lamination force exacerbated compression failures under high drift loading once laminations split apart. Figure 16 shows the split resulting from this type of failure mode.

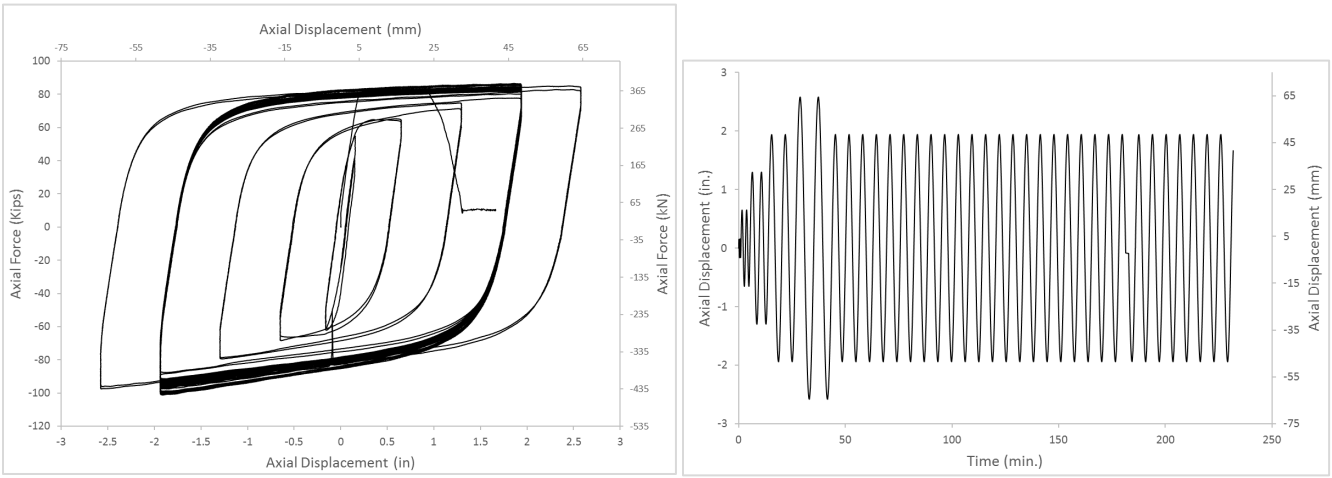

Figure 9. Specimen 1: hysteresis (left) and displacement vs time (right).

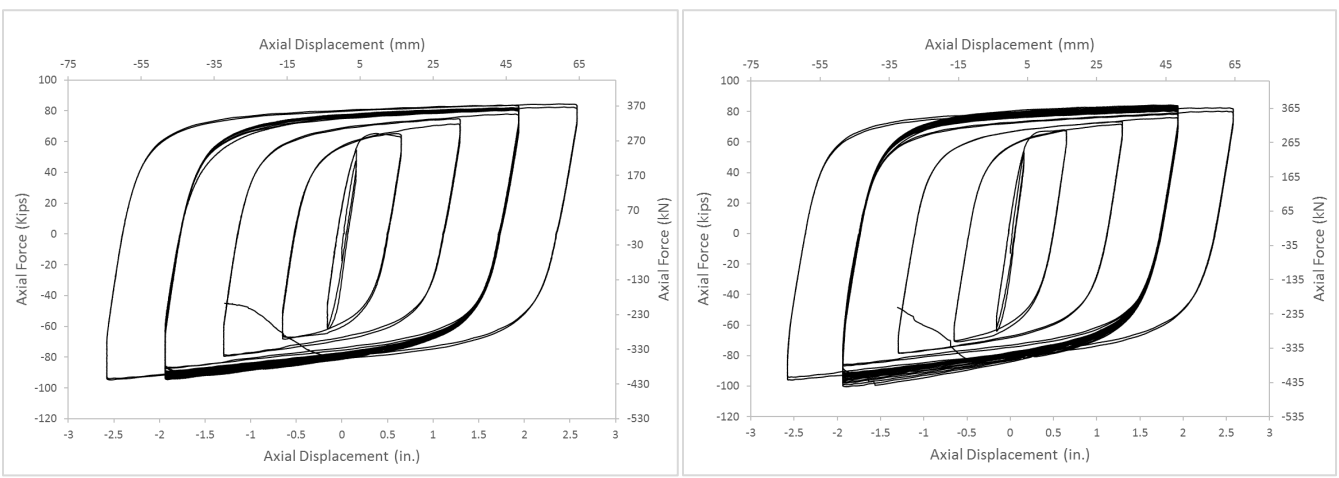

Figure 10. Specimen 2 (left) and Specimen 3 (right) hysteresis.

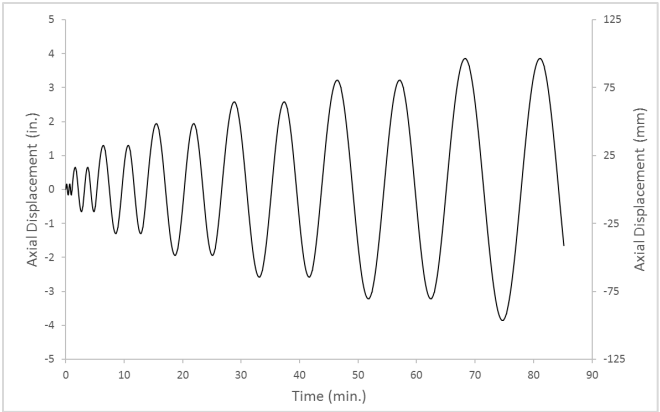

Figure 11: Specimen 4: hysteresis (left) and displacement vs time (right).

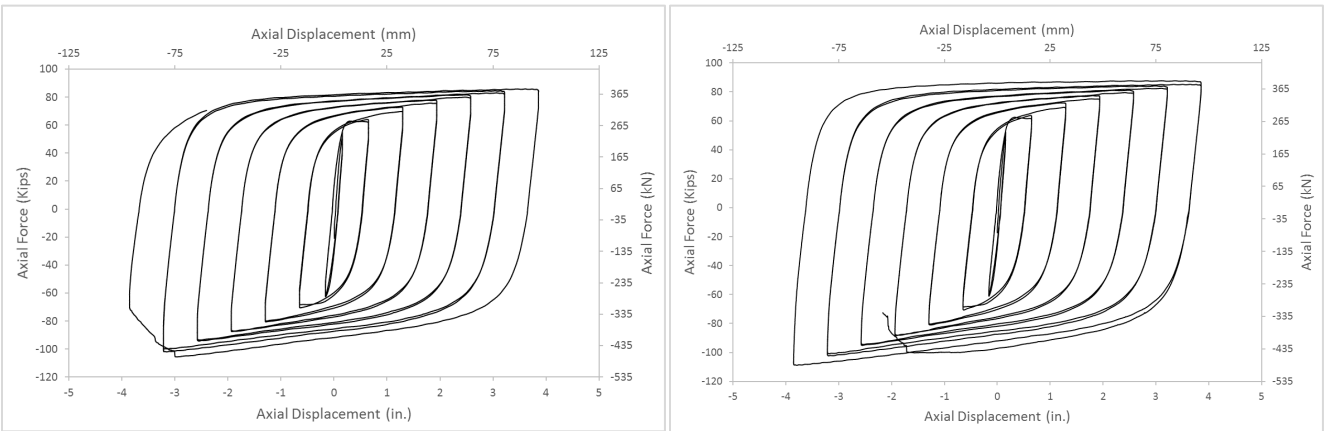

Figure 12: Specimen 5 (left) and Specimen 6 (right) hysteresis.

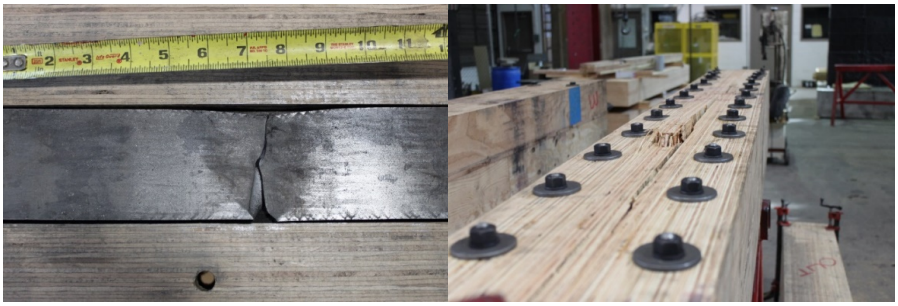

Figure 13. Failure mode of Specimen 1 (left) and Specimen 2 (right).

Figure 14. Failure mode of Specimen 3 (left) and Specimen 4 (right).

Figure 15. Failure mode of Specimen 5 (left) and Specimen 6 (right).

Figure 16. MPP casing split resulting from strong axis steel core buckling.

6 Conclusions

This research demonstrated that a reliable and efficient T-BRB is possible to construct and feasible to implement when combining a steel core with an engineered timber casing. The following conclusions can be drawn:

1. Unreinforced Glulam underperforms when compared to other engineered wood products; this wood type consistently fails before reaching 0.1in. of displacement when loaded in the parallel to lamination direction.
2. MPP loaded perpendicular to laminations without screw reinforcement also underperforms compared to MPP loaded parallel to laminations when considering elastic stiffness. Average elastic stiffness of perpendicular loaded samples resulted in 77 kip/in. while parallel loaded samples resulted in 257 kip/in.
3. The T-BRBs tested in this research using MPP loaded parallel to grain meet the requirements of ASCE-341-16. The hysteresis curves from these specimens prove that sufficient energy dissipation is readily achievable with a T-BRB.
4. Specimens 1-6 reached cumulative inelastic deformations of 1571, 1416, 1107, 580, 488, and 580 times the yield deformation, respectively which exeeds ASCE 341-16 requirements for ductility corresponding to 2.0 times the design story drift and a cumulative inelastic axial ductility of 200 times the yield displacement.
5. The hysteretic curves prove stable damping is possible with T-BRBs.

6. A 3.9% strain was sustained under the drift-based loading protocol. The T-BRB has a long fatigue life at 1.5% strain, as shown for the fatigue tested T-BRB specimens.
7. The compressive adjustment factor, β, remained below 1.5 per AISC 341-16 for all specimens; this factor ranged from between 1.05 to 1.25. The strain hardening adjustment factor, ω exceeded 1.0 per AISC 341-16 for all specimens and ranged from 1.00 to 1.43.

7 References

American Institute of Steel Construction - AISC 341 (2016): *Seismic provisions for Structural Steel Buildings*, Chicago, Illinois.

Bader, T, Schweigler, M, Hochreiner, G, and Eberhardsteiner, J (2016): Load Distribution in Multi-dowel Timber Connections under Moment Loading-Integrative Evaluation of Multiscale Experiments. *World Conference on Timber Engineering,* 2016. Vienna, Austria.

Black, CJ, Makris, N, and Aiken, ID (2004): Component Testing, Seismic Evaluation and Characterization of Buckling-Restrained Braces. *Journal of Structural Engineering*, 130(6), 880–894.

Blass HJ, and Bejtka I (2003): Reinforcements Perpendicular to Grain Using Self-Tapping Screws. University of Karlsruhe, Karlsruhe, Germany.

Blomgren, H, Koppitz, J, Valdes, A and Ko, E (2016): The Heavy Timber Buckling-Restrained Braced Frame as a Solution for Commercial Buildings in Regions of High Seismicity. Vienna, Austria: WCTE.

Genna, F, and Gelfi, P (2012): Analysis of the Lateral Thrust in Bolted Steel Buckling-Restrained Braces. II: Engineering Analytical Estimates." *Journal of Structural Engineering*, 138(10), 1244–1254.

Lin, P-C, et al. (2011): Seismic design and hybrid tests of a full-scale three-story buckling-restrained braced frame using welded end connections and thin profile. *Earthquake Engineering & Structural Dynamics*, 41(5), 1001–1020.

Popovski, M (2000): Seismic Performance of Braced Timber Frames. Ph. D. thesis, Department of Civil Engineering, the University of British Columbia, Vancouver, B.C.

Watanabe, A, Hitomoi Y, Saeki E, Wada A, and Fujimoto M (1988): Properties of Brace Encased in Buckling-Restraining Concrete and Steel Tube. *Proceedings of the 9th World Conference on Earthquake Engineering, Tokyo-Kyoto, Japan,* 719-724.

Wu, A-C, Lin, P-C, and Tsai, K-C (2013): High-mode buckling responses of buckling-restrained brace core plates. *Earthquake Engineering & Structural Dynamics*, 43(3), 375–393.

View publication stats